Cell, Vol. 112, 549–560, February 21, 2003, Copyright ©2003 by Cell Press

Adenylyl Cyclase Localization Regulates Streaming during Chemotaxis

Paul W. Kriebel, Valarie A. Barr, and Carole A. Parent*
Laboratory of Cellular and Molecular Biology
Center for Cancer Research
National Cancer Institute
National Institutes of Health
37 Convent Drive
Building 37/Room 1E24
Bethesda, Maryland 20892

Summary

We studied the role of the adenylyl cyclase ACA in *Dictyostelium discoideum* chemotaxis and streaming. In this process, cells orient themselves in a head to tail fashion as they are migrating to form aggregates. We show that cells lacking ACA are capable of moving up a chemoattractant gradient, but are unable to stream. Imaging of ACA-YFP reveals plasma membrane labeling highly enriched at the uropod of polarized cells. This localization requires the actin cytoskeleton but is independent of the regulator CRAC and the effector PKA. A constitutively active mutant of ACA shows dramatically reduced uropod enrichment and has severe streaming defects. We propose that the asymmetric distribution of ACA provides a compartment from which cAMP is secreted to locally act as a chemoattractant, thereby providing a unique mechanism to amplify chemical gradients. This could represent a general mechanism that cells use to amplify chemotactic responses.

Introduction

Chemotaxis is a process by which cells orient themselves and move up a chemical gradient. It is important in a variety of physiological and pathological processes including nerve growth, angiogenesis, wound healing, carcinoma invasion, and leukocyte trafficking. It is also essential for the survival of the social amoebae *Dictyostelium discoideum* (Aubry and Firtel, 1999; Parent and Devreotes, 1996b). When starved, these amoebae enter a differentiation program that allows the cells to survive harsh environmental conditions. They do so by chemotaxing toward secreted adenosine 3′, 5′ cyclic monophosphate (cAMP) signals thereby forming aggregates that differentiate into spores supported by a stalk of vacuolated cells. The essential role of chemotaxis in this eukaryote makes it an excellent model organism to study the biochemical and genetic basis of directed cell migration (Chung et al., 2001a; Parent and Devreotes, 1999).

For both leukocytes and *D. discoideum* amoebae, chemotactic responses are mediated via G protein-coupled receptors. Upon activation of the receptors, the G proteins dissociate into α and $\beta\gamma$ subunits and these two entities activate, either alone or in concert, a variety of responses, including increases in the proportion of polymerized actin and the stimulation of adenylyl cyclase. A mechanism to explain how signaling is spatially restricted in chemotaxing cells emerged when it was shown that the PH domain-containing *D. discoideum* protein CRAC (*c*ytosolic *r*egulator of *a*denylyl *c*yclase) translocates from the cytoplasm to the plasma membrane exclusively at the leading edge of chemotaxing cells (Parent et al., 1998). A similar translocation was later shown with other PH domain-containing proteins, including Akt/PKB, in both *D. discoideum* and neutrophils (Meili et al., 1999; Servant et al., 2000). Since both chemoattractant receptors and heterotrimeric G proteins were shown to be mostly uniformly distributed at the periphery of chemotaxing cells, it was proposed that chemotaxing cells localize signaling events at their leading edge by spatially generating binding sites for PH domain-containing proteins, which would then locally control the actin assembly (Jin et al., 2000; Parent and Devreotes, 1999; Servant et al., 1999; Xiao et al., 1997).

Biochemical and genetic analyses have established that receptor and GTPγS activation of the adenylyl cyclase ACA in *D. discoideum* requires the $\beta\gamma$ subunit of heterotrimeric G proteins and CRAC, but the mechanisms by which this occurs remain to be established. Activation of chemoattractant receptors leads to the dissociation of the heterotrimeric G proteins and the translocation of CRAC to the plasma membrane (Insall et al., 1994; Lilly and Devreotes, 1995; Wu et al., 1995). This series of events then leads to the activation of ACA and cAMP is produced. In *D. discoideum*, a large proportion of cAMP is secreted and acts as a chemoattractant by binding to G protein-coupled cAMP receptors (cARs, *c*yclic *A*MP *r*eceptors). The binding of cAMP to cARs activates a multitude of signaling pathways giving rise to chemotaxis, the synthesis and secretion of additional cAMP for signal relay and changes in gene expression (Aubry and Firtel, 1999). Consequently, cells lacking Gβ, CRAC, or ACA cannot produce cAMP in response to receptor stimulation and therefore remain as non-aggregating smooth monolayers of cells when deprived of nutrients (Insall et al., 1994; Pitt et al., 1992; Wu et al., 1995). Interestingly, in some mammalian cells, including neutrophils, a large proportion of cAMP is also secreted, although the exact function of the extracellular cAMP is unknown at this time (Harvath et al., 1991).

In order to gain more insight into the signaling events involved in directed cell migration, we studied the mechanisms by which *D. discoideum* amoebae use cAMP to regulate cell migration using two approaches. First, the chemotactic behavior of *D. discoideum* cells lacking the adenylyl cyclase ACA was determined. Second, we used the GFP technology to study the localization of adenylyl cyclase in live chemotaxing cells. We found that although ACA is not required for chemotaxis, it is essential for cells to align in a head to tail fashion and stream into aggregates. We suggest that this occurs because ACA is highly enriched at the back of migrating cells

*Correspondence: parentc@helix.nih.gov

thereby providing a compartment from which cAMP is secreted and acts as a chemoattractant.

Results

aca⁻ Cells Have Polarity Defects and Do Not Stream

In an attempt to understand the role of adenylyl cyclase in the establishment of polarity as well as chemotaxis, we examined the properties of cells lacking the adenylyl cyclase ACA. These experiments were performed on cells that were treated with cAMP every 6 min for 5–7 hr, which mimics normal developmental cAMP signaling and bypasses the cAMP production defect of *aca*⁻ cells. Under these conditions, *aca*⁻ cells express developmental genes including chemoattractant receptors at normal levels and with typical kinetics (data not shown; Pitt et al., 1993). Moreover, differentiated *aca*⁻ cells display normal chemoattractant-stimulated guanylyl cyclase activity and properly generate CRAC binding sites on their plasma membrane in the presence of chemoattractant or GTPγS (Lilly and Devreotes, 1995; Pitt et al., 1992). Despite this, in the absence of chemoattractant, we find that *aca*⁻ cells behave differently than wild-type cells. Whereas wild-type cells exhibit a polarized shape and are motile, *aca*⁻ cells display a severe defect in polarity and remain virtually immobile (see Supplemental Movies S1 and S2 available at http://www.cell.com/cgi/content/full/112/4/549/DC1). We further compared the behavior of these cells by placing them in a spatial gradient generated by a micropipette filled with chemoattractant. The top images of Figure 1A (0 time point) were taken before the chemoattractant was delivered by the micropipette. Within seconds after activating the micropipette, the polarized wild-type cells rapidly sense the gradient and exhibit robust chemotaxis (Figure 1A and Supplemental Movie S3 available at above website). The *aca*⁻ cells, on the other hand, do not immediately migrate to the tip of the micropipette. Instead, they initially respond to the gradient by acquiring a polarized shape. Subsequently, after a short lag, the now polarized *aca*⁻ cells efficiently chemotax to the tip of the micropipette (Figure 1A and Supplemental Movie S4 available at above website). Furthermore, once polar and properly chemotaxing, *aca*⁻ cells are able to extend pseudopods from their original migrating fronts and turn in response to abrupt changes in chemoattractant gradients. Figure 1B shows a montage of images captured as *aca*⁻ cells are turning in response to a change in the position of the micropipette.

The fact that the *aca*⁻ cells become polarized and mobile when exposed to a chemoattractant gradient reminded us of the well-established chemokinesis property of neutrophils in which cells stimulated with a uniform increase of chemoattractant polarize and start to randomly move (Hauert et al., 2002; Zigmond et al., 1981). We therefore asked if *aca*⁻ cells would respond similarly and therefore share this characteristic with neutrophils. As shown in Figure 1C and Supplemental Movie S5 (available at above website), moments after the uniform addition of 10 nM cAMP, the *aca*⁻ cells went from being mostly spherical and stationary to polarized and motile. When plated at standard cell density (15 cells/100 μm^2), wild-type cells do not display this chemokinesis behavior, presumably because they have endogenous adenylyl cyclase activity that generates enough cAMP to induce the chemokinesis response. However, when we decreased the cell density to 2 cells/100 μm^2, wild-type cells appeared non-polarized and immobile. After the addition of a uniform amount of chemoattractant, the cells responded and became polarized and motile much like the *aca*⁻ cells did (data not shown). These results show that, like neutrophils, *D. discoideum* amoebae require chemoattractant stimulation to acquire polarity, a prerequisite for the development of migration.

Once wild-type cells have begun chemotaxing to a point source of cAMP, they eventually organize into streams that are composed of cells migrating in a head to tail fashion. The streams come together generating characteristic star-like patterns. As shown in Figure 1D, *aca*⁻ cells are incapable of generating streams, even after a prolonged time in a chemoattractant gradient. Consequently, while not essential for chemotaxis, the signal relay response involving the binding of cAMP to cARs and the subsequent activation of ACA is clearly required for the streaming process.

ACA-YFP Localizes to the Uropod of Polarized Chemotaxing Cells

In order to gain more insight into the function of ACA in polarity and streaming, we fused YFP to ACA and visualized the cellular distribution of ACA in live cells. To test the functionality of the ACA-YFP fusion protein, we transformed *aca*⁻ cells with the ACA-YFP expression plasmid and assessed the developmental phenotype of the resultant transformants on non-nutrient agar. Expression of ACA-YFP in *aca*⁻ cells (ACA-YFP/*aca*⁻) rescued the aggregation-deficient phenotype of the *aca*⁻ cells (Figure 2A, inset). Moreover, Western analysis showed that the cells expressed the expected ~170 kDa fusion product exclusively in the membranous pellet fraction (data not shown). The enzymatic activity of ACA-YFP in response to receptor activation was determined by performing adenylyl cyclase assays. In these assays, intact cells are stimulated with chemoattractant and at specific time points the adenylyl cyclase activity is measured in lysates. Whereas *aca*⁻ cells had no detectable adenylyl cyclase activity upon receptor activation, the ACA-YFP/*aca*⁻ cells showed the characteristic rapid rise in enzyme activity followed by a slow return to basal levels (Figure 2A). Taken together, these results demonstrate that the ACA-YFP fusion protein has retained wild-type-like properties.

We studied the cellular distribution of ACA-YFP in differentiated, chemotaxis-competent cells. Remarkably, we observed that the plasma membrane distribution of ACA-YFP in these polarized and differentiated cells was strongly asymmetric with one end of the cells showing a much brighter fluorescent signal (Figure 2B). This enrichment was also observed in thin 1 μm confocal sections, thereby excluding the possibility that this clustering was due to membrane ruffling. Several experiments were performed to rule out that the asymmetric distribution of ACA-YFP was an artifact. First, we generated and compared cell lines in which the amount and enzymatic activity of ACA-YFP varied by a factor of ~10. As can be seen in Figure 2B, *aca*⁻ cells expressing both

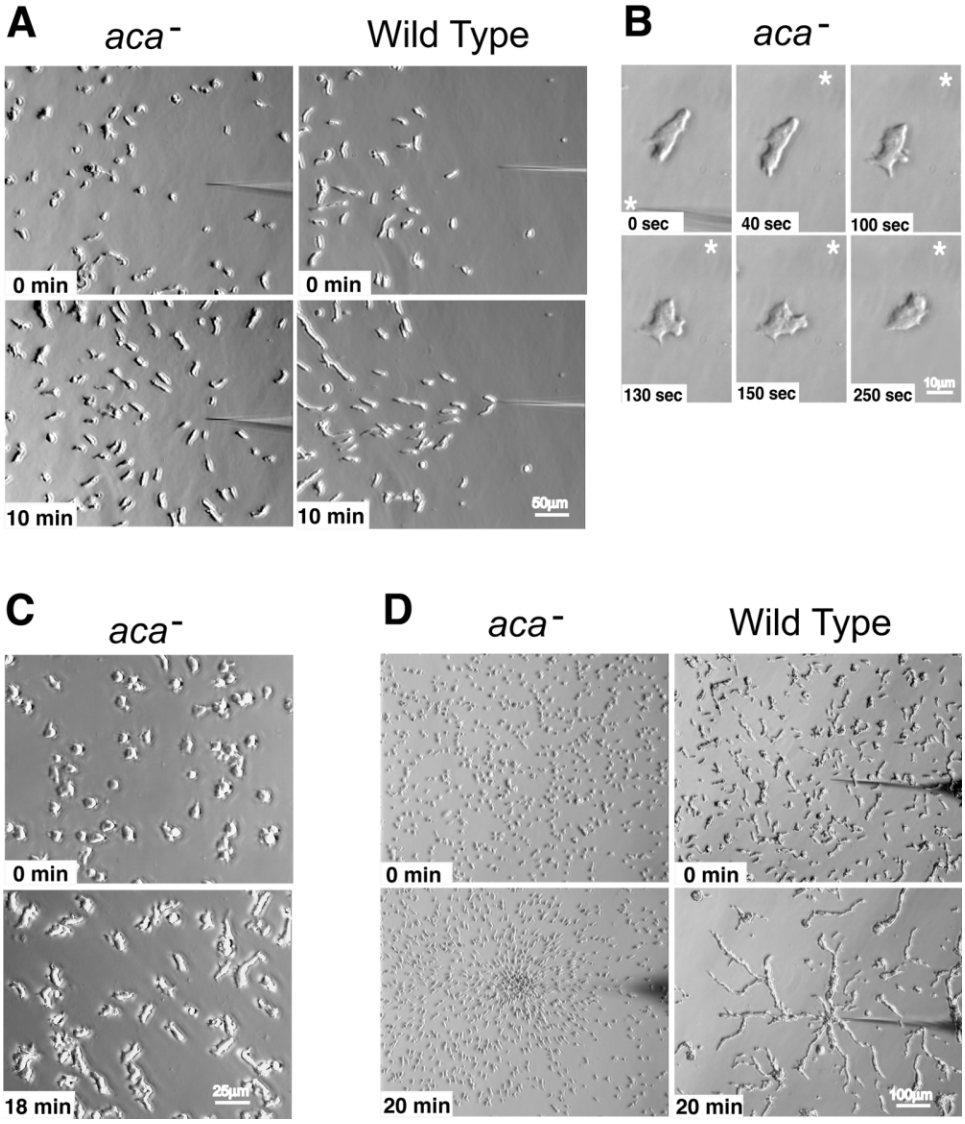

Figure 1. *aca*⁻ Cells Chemotax but Do Not Stream

(A) Images of *aca*⁻ and wild-type AX3 cells moving toward a micropipette filled with chemoattractant. Also see Supplemental Movie S3 (wild-type) and Supplemental Movie S4 (*aca*⁻) available at http://www.cell.com/cgi/content/full/112/4/549/DC1.

(B) Images of *aca*⁻ cells turning in response to an abrupt change in the position of the chemoattractant gradient. The micropipette was moved as depicted by the star at 30 s.

(C) Images of *aca*⁻ cells just before and 18 min after the cells were subjected to 10 nM cAMP (uniform increase). Also see Supplemental Movie S5 available at above website.

(D) Low magnification images of *aca*⁻ and wild-type AX3 cells moving toward the micropipette.

high and low levels of ACA-YFP clearly display the asymmetric plasma membrane distribution. Second, indirect immunofluorescence demonstrated that untagged ACA was also clustered on the plasma membrane (Figure 2C).

To determine if the cluster of ACA is present at the leading edge or the uropod of chemotaxing cells, fully differentiated ACA-YFP/*aca*⁻ cells were placed in a gradient of chemoattractant. We found that ACA-YFP was enriched at the uropod of chemotaxing cells (Figure 2D and Supplemental Movie S6 available at http://www.cell.com/cgi/content/full/112/4/549/DC1). As expected, when we changed the position of the micropipette, these highly differentiated cells extended pseudopods from their original migrating front and turned toward the newly established gradient thereby maintaining their original polarity with ACA-YFP at the back (data not shown). Very interestingly, when this same experiment is performed on cells that were starved for only 4 hr and thus incompletely polarized, we often observed cells extending new pseudopods from their back while locally maintaining strong ACA-YFP labeling (Figure 2E). It therefore appears that ACA-YFP enrichment at the back identifies a domain that possesses specific properties.

ACA-YFP Also Labels Intracellular Vesicles

Closer examination of ACA-YFP/*aca*⁻ cells using confocal microscopy imaging revealed that, in addition to labeling the plasma membrane, ACA-YFP localized to

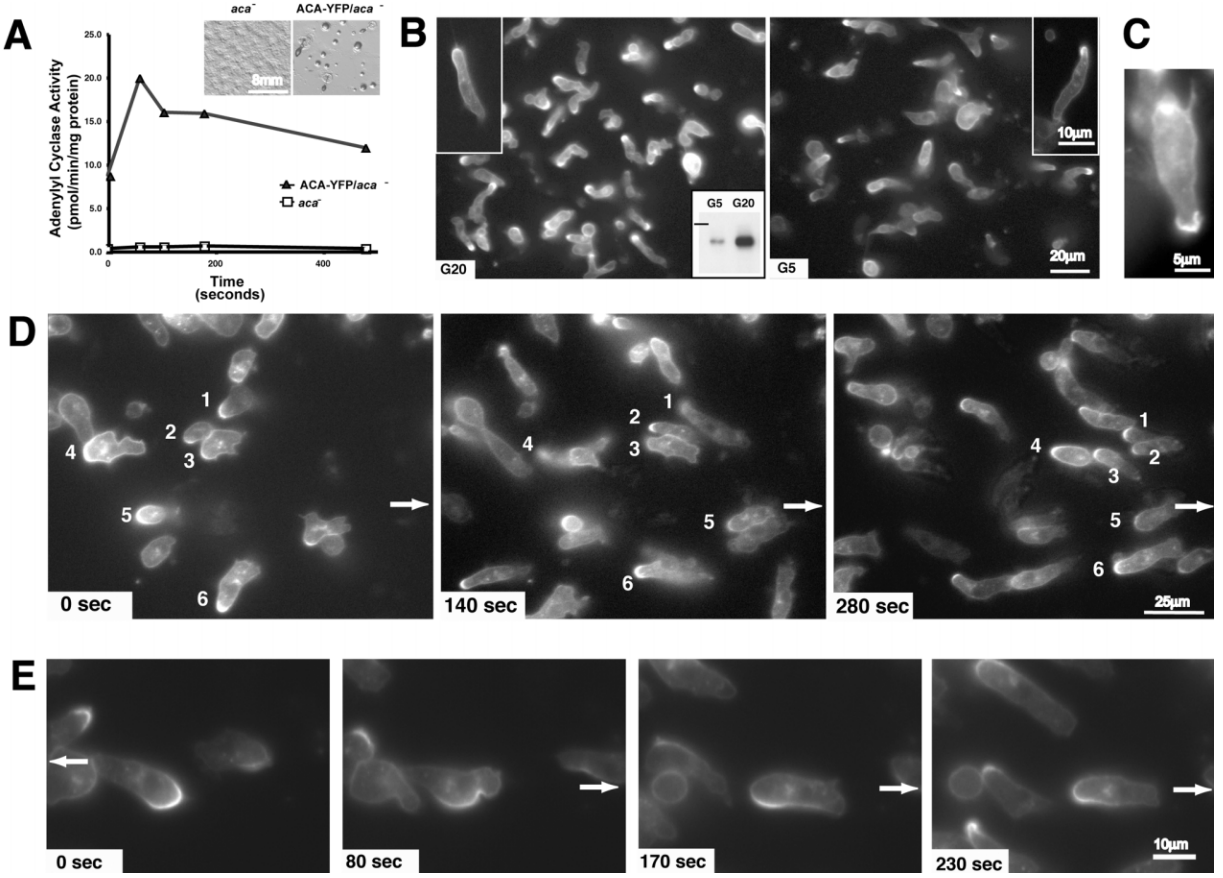

Figure 2. ACA-YFP Behaves Like Wild-Type ACA and Is Enriched at the Back of Chemotaxing Cells

(A) Adenylyl cyclase activity measured following chemoattractant stimulation. Differentiated cells were stimulated with 10 μM cAMP, and at specific time points, aliquots were lysed and the adenylyl cyclase activity was measured for 1 min. These results are representative of at least 5 independent experiments. The inset shows the developmental phenotype of *aca*⁻ and ACA-YFP/*aca*⁻ cells on non-nutrient agar. Photographs were taken 24 hr after the cells were plated.

(B) Fluorescent images of ACA-YFP/*aca*⁻ cells selected using 5 μg/ml G418 (G5) or 20 μg/ml G418 (G20) after 5 hr of starvation. A high magnification image is also presented for each cell line. The inset shows Western analysis of whole cells harvested from both cell lines using an antibody directed against GFP. The bar represents the 200 kDa marker.

(C) Indirect fluorescent image of differentiated ACA/*aca*⁻ cells. Cells were fixed and stained with anti-ACA antibody.

(D) Montage of fluorescent images depicting ACA-YFP/*aca*⁻ cells chemotaxing in a gradient of chemoattractant. The arrow indicates the position of the tip of the micropipette. Cells are individually numbered as they move up the gradient. Also see Supplemental Movie S6 available at http://www.cell.com/cgi/content/full/112/4/549/DC1.

(E) Fluorescent images of ACA-YFP/*aca*⁻ cells differentiated for 4 hr, as they are chemotaxing in a gradient of chemoattractant. The micropipette was moved as depicted by the arrow at 30 s.

intracellular vesicles (see Supplemental Movie S7 available at above website). Many labeled vesicles showing rapid dynamic movement can be seen in these differentiated ACA-YFP/*aca*⁻ cells. As was the case for the uropod labeling, this distribution was observed in cells expressing both high and low levels of ACA-YFP (Figure 2B). To rule out that the vesicles were part of the lysosomal pathway, we exposed the cells to a dye that specifically labels lysosomes (Lysotracker). As seen in Supplemental Movie S8 (available at above website), the ACA-YFP (in green) and Lysotracker (in red) signals did not colocalize. These results suggest that the intracellular vesicles are not delivering ACA to lysosomes for degradation. Therefore, it is possible that ACA is being specifically transported, perhaps as part of a signal transduction pathway.

The Asymmetric Distribution of ACA-YFP Is Dependent on the Actin Cytoskeleton and on the Acquisition of Cellular Polarity

To gain more insight into the mechanisms that regulate how ACA-YFP is enriched at the uropod of cells, we studied the distribution of ACA-YFP at various times after the onset of starvation as the cells acquire polarity (Figure 3A). In their non-differentiated, vegetative state, the amoebae are round and show little polarity. However, as they starve and differentiate, the cells elongate, so that after ~5 hr of starvation they exhibit a highly polarized shape. At the initiation of starvation, ACA-YFP/*aca*⁻ cells display a uniform fluorescent signal at their surface (Figure 3A, 0 time point). As the cells differentiate and polarize, the ACA-YFP signal becomes asymmetrically distributed on the plasma membrane,

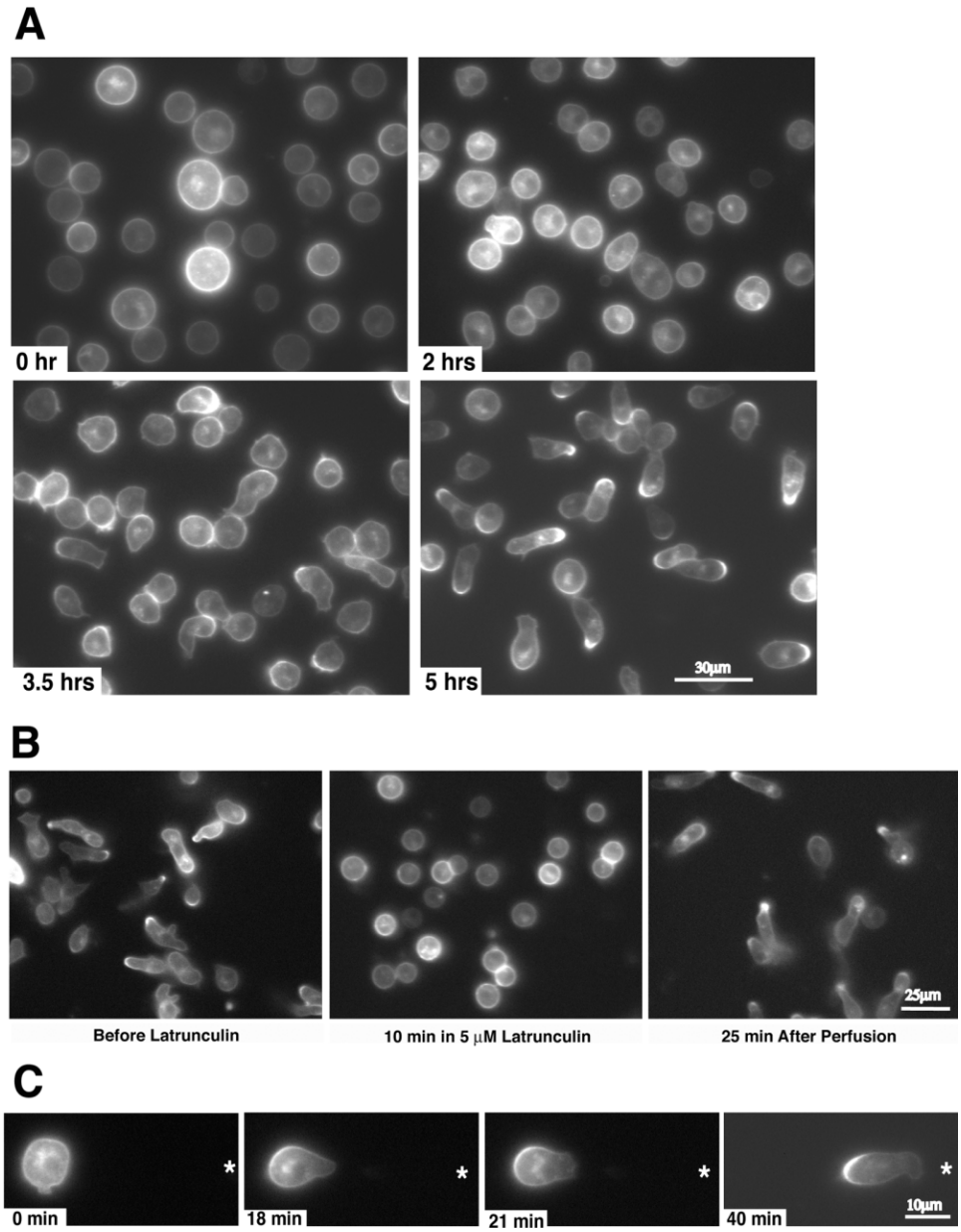

Figure 3. The Asymmetric Distribution of ACA-YFP Is Dependent on the Actin Cytoskeleton and the Acquisition of Cellular Polarity

(A) Fluorescent images of ACA-YFP/*aca*$^-$ cells. The numbers in the bottom corners represent hours after the initiation of starvation.

(B) Fluorescent images of ACA-YFP/*aca*$^-$ cells before, 10 min after the addition of 5 μm latrunculin, and 25 min after the removal of latrunculin.

(C) Fluorescent images of ACA-YFP/*aca*$^-$ cells plated at low density and exposed to a chemoattractant gradient. Star indicates the position of the micropipette.

so that at ~5 hr of starvation, the signal is highly enriched (Figure 3A, 2, 3.5, and 5 hr time points).

We next tested if the enrichment of ACA-YFP at the uropod was dependent on the actin cytoskeleton using the inhibitor of actin polymerization, latrunculin A. Minutes after the addition of the drug, cells become progressively round and within ~10 min most of them virtually stop moving. Under these conditions, the distribution of ACA-YFP on the plasma membrane changes from being enriched at the uropod to perfectly uniform (Figure 3B). This effect is not only rapid but it is also completely reversible. Upon removal of the drug, the cells quickly regain their polarized state and ACA-YFP clusters on the plasma membrane (Figure 3B). A similar phenomenon occurs when we plate fully differentiated ACA-YFP/*aca*$^-$ cells at low density. Under these conditions, the cells are apolar and the ACA-YFP signal is uniformly distributed (Figure 3C, 0 time point). However, when we expose the cells to a chemoattractant gradient, they respond by extending a pseudopod up the gradient and acquiring a polarized shape. Concomitantly, the ACA-YFP signal becomes enriched at the uropod (Figure 3C). These results show that (1) the asymmetric distribution of ACA-YFP depends on the actin cytoskeleton and (2) chemoat-

tractant stimulation induces cellular polarity and the asymmetric distribution of ACA.

Our data support the hypothesis that the asymmetric distribution of ACA-YFP depends on the acquisition of cellular polarity. But the presence of ACA at the uropod of cells is not essential for cells to polarize. As shown in Figure 1A, cells lacking ACA display robust chemotaxis and polarize when exposed to chemoattractants. Furthermore, the *aca*$^-$ cells extend pseudopods from their original migrating fronts and turn in response to abrupt changes in chemoattractant gradients (Figure 1B). Taken together, these results establish that the enrichment of ACA at the back of chemotaxing cells occurs as a result of cellular polarity and that ACA itself has little or no role in the establishment of polarity per se.

Signaling Events Leading to the Asymmetric Distribution of ACA

Since the activation of ACA requires the cytosolic regulator CRAC, we studied the role of CRAC in the cellular distribution of ACA-YFP (Insall et al., 1994). We expressed ACA-YFP in *crac*$^-$ cells and studied its cellular distribution in differentiated cells. As seen in Figure 4A, the ACA-YFP signal is asymmetrically distributed in *crac*$^-$ cells much like what we observe in a wild-type setting. To further this analysis, we studied the distribution of CRAC in cells lacking ACA. As we had observed in wild-type cells, we found that CRAC-GFP localized to the leading edge when expressed in *aca*$^-$ cells (Figure 4B). Furthermore, in contrast to what we have shown for ACA, it has been established that the translocation of CRAC to the plasma membrane is not dependent on the actin cytoskeleton (Parent et al., 1998). These results show that CRAC is not required for ACA to localize to the uropod and that the mechanism(s) responsible for the cellular localization of ACA and CRAC are most probably independent.

We next evaluated the role of PKA, the main cellular target of cAMP, on the distribution of ACA. We transformed ACA-YFP in cells lacking the catalytic subunit of PKA (*pkacat*$^-$) and selected stable transformants. We found that ACA-YFP is asymmetrically distributed in some starved and pulsed cells (Figure 4C). However, since PKA is involved in the expression of several developmental genes, a significant number of cells did not acquire a polarized shape and did not exhibit a strong uropod enrichment. Indeed, it has been shown that constitutive expression of ACA in *pkacat*$^-$ cells does not restore normal development (Mann et al., 1997). To overcome this drawback, we treated fully differentiated ACA-YFP/*aca*$^-$ cells with the PKA inhibitor H89 and found that it did not alter the asymmetric distribution of ACA-YFP (Figure 4D; Anjard et al., 1997). Similarly, constitutive activation of PKA did not alter the distribution since ACA-YFP/*aca*$^-$ cells treated with 8-bromo-cAMP, a cAMP homolog that preferentially activates PKA, show wild-type-like distribution (Figure 4E; van Ments-Cohen and van Haastert, 1989; Brickey et al., 1990). These results establish that PKA or its state of activation are not involved in regulating the cellular distribution of ACA.

A Constitutive Mutant of ACA Shows Aberrant Cellular Distribution

To investigate the requirement for enzymatic activity in the localization of ACA, we fused YFP to ACA mutants

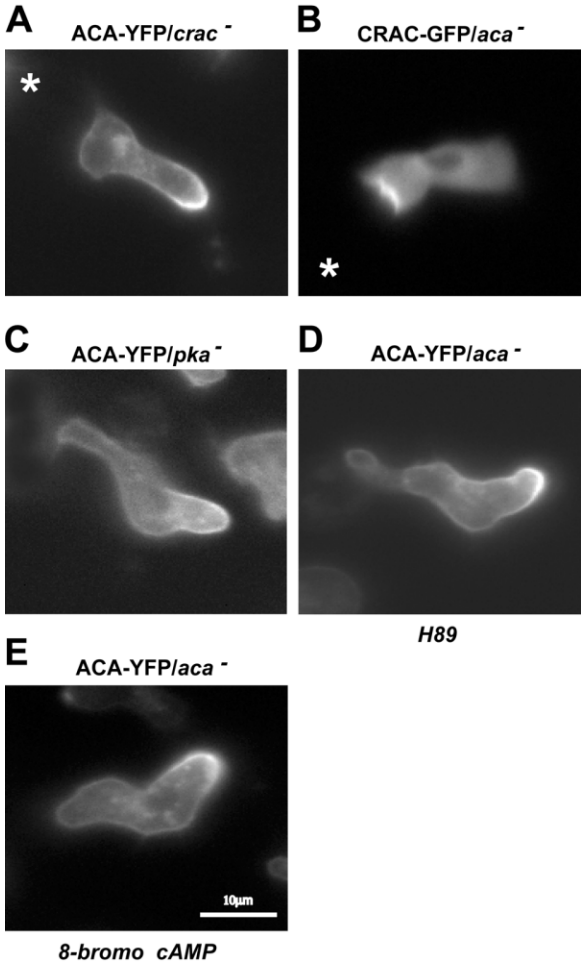

Figure 4. CRAC and PKA Are Not Involved in Controlling the Cellular Distribution of ACA

The ACA-YFP plasmid was electroporated in *crac*$^-$ and *pkacat*$^-$ cells and stable transformants were selected. Similarly, *aca*$^-$ cells expressing CRAC-GFP were generated. The cell lines were differentiated and the cellular distribution of ACA-YFP or CRAC-GFP analyzed by fluorescent microscopy (A, B, and C).

(D and E) Differentiated ACA-YFP/*aca*$^-$ cells were treated with 50–500 nM of H-89 or up to 8 mM 8-bromo-cAMP and fluorescent images were captured.

that had either lost the capacity to be activated by G proteins (uncoupled-U) or were constitutively active (C). Both mutants were previously isolated using genetic screens and harbored single amino acid substitutions within the first cytoplasmic loop (Parent and Deveotes, 1995, 1996a). As expected, the uncoupled mutant (ACA-U-YFP) did not rescue the aggregation-deficient phenotype of the *aca*$^-$ cells and was not activated by GTPγS. The constitutive mutant (ACA-C-YFP) exhibited high basal activity that was further stimulated by activated G proteins and, as previously shown with the untagged version, rescued the developmental defect of the *aca*$^-$ cells (Figure 5A). Both mutants were expressed at levels that were similar to the wild-type enzyme (Figure 5A, inset).

The uncoupled and constitutive mutants showed different cellular distributions. Whereas the uncoupled mutant was asymmetrically distributed, akin to its wild-

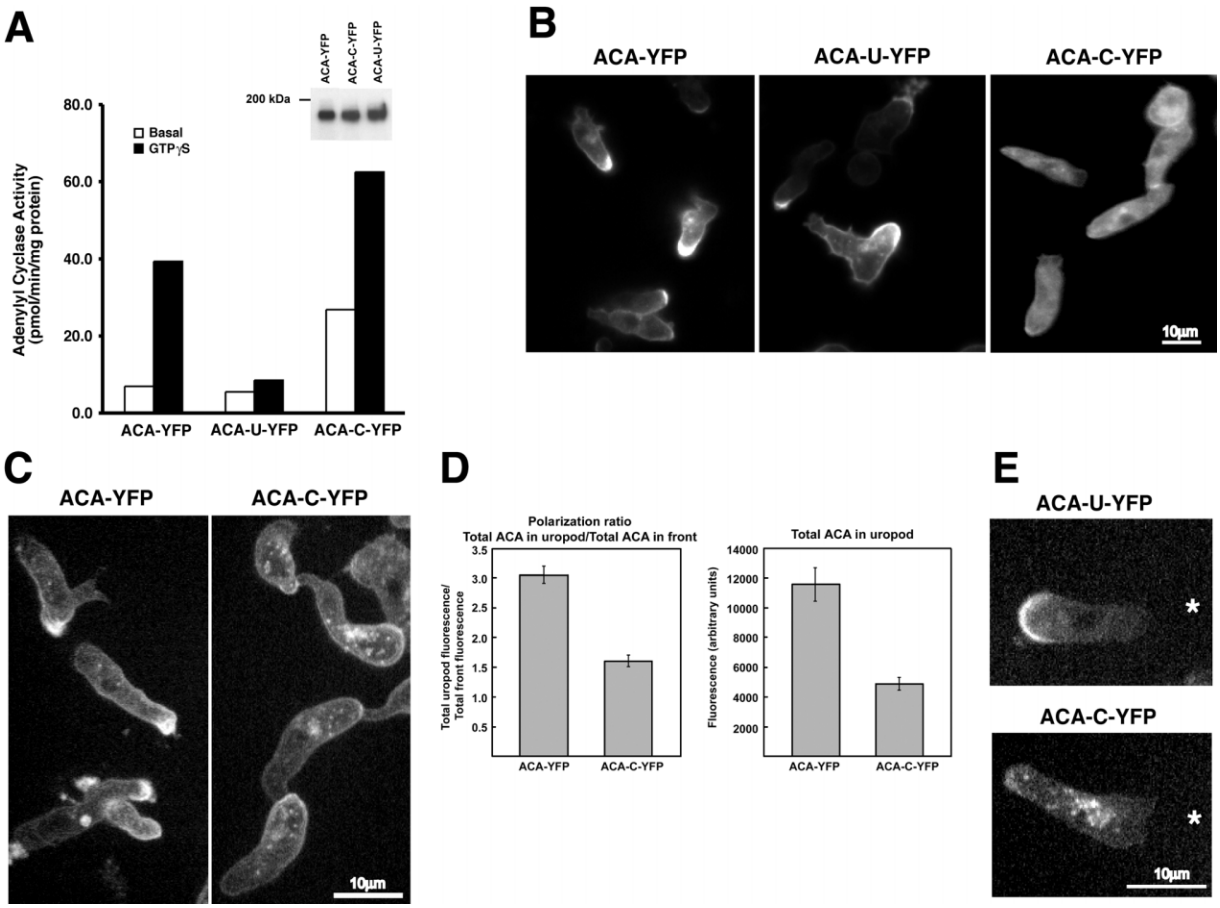

Figure 5. A Constitutive Mutant of ACA Shows Aberrant Cellular Localization

(A) Basal and G protein-mediated (40 μM GTPγS) activation of adenylyl cyclase of wild-type (ACA-YFP), uncoupled (ACA-U-YFP), and constitutively active (ACA-C-YFP) mutants of ACA. These results are representative of at least 3 independent experiments. The inset shows a Western analysis of whole cells derived from the various cell lines.

(B) Montage of fluorescent images depicting differentiated ACA-YFP/*aca*$^-$, ACA-U-YFP/*aca*$^-$, and ACA-C-YFP/*aca*$^-$ cells.

(C) Montage of confocal fluorescent images depicting differentiated ACA-YFP/*aca*$^-$ and ACA-C-YFP/*aca*$^-$ cells.

(D) The two bar graphs depict the fluorescence intensity measured at the uropod over the intensity measured at the front of cells and the total amount of fluorescence measured at the uropod, respectively (n = 48 for ACA-YFP and 49 for ACA-C-YFP).

(E) Montage of confocal fluorescent images depicting differentiated ACA-U-YFP/*aca*$^-$ and ACA-C-YFP/*aca*$^-$ cells migrating in a chemoattractant gradient. The stars represent the position of the tip of the micropipette. For (C) and (E), images were taken with the Ultra View spinning disk confocal system. Each image is a maximum intensity projection of 5 to 8, 1 μm sections.

type counterpart, the constitutive mutant displayed a dramatically reduced enrichment at the back (Figure 5B). To further study this, we acquired confocal images of cells expressing the wild-type and the constitutively active mutant and performed quantitative analyses of the fluorescence intensity measured at the back and front of cells (Figure 5C). Because of the peculiar distribution of ACA-C-YFP, quantification was restricted to a small area of the plasma membrane at the uropod of mutant and wild-type-expressing cells (see Experimental Procedures), a strategy that may have significantly underestimated the enrichment of the wild-type enzyme. Nevertheless, we found that cells expressing wild-type ACA have on average greater than 3 times more ACA at their back, compared to 1.5 times for the constitutive mutant (Figure 5D). Furthermore, cells expressing wild-type ACA display 2.4 times more total fluorescence at their back compared to cells expressing the constitutive mutant. Given that both cell lines express a comparable amount of total protein (Figure 5A, inset), this shows that there are significantly more ACA molecules at the back of wild-type cells. In addition to the reduced enrichment at the back, we also observe that the constitutive mutant displays a higher number of intracellular vesicles (Figure 5C). When we placed the mutant cells lines in a gradient of chemoattractant, they all chemotaxed and the aberrant cellular distribution of the constitutive mutant was retained (Figure 5E). These results show that the cellular distribution of ACA is dependent on the state of activation of the enzyme, whereby high constitutive activity leads to a considerable change in the amount of ACA that is present in the plasma membrane and vesicular pools, respectively.

The Localization of ACA at the Uropod Is Essential for Streaming

The observations that ACA is essential for streaming and that it is enriched at the uropod suggest a mechanism to

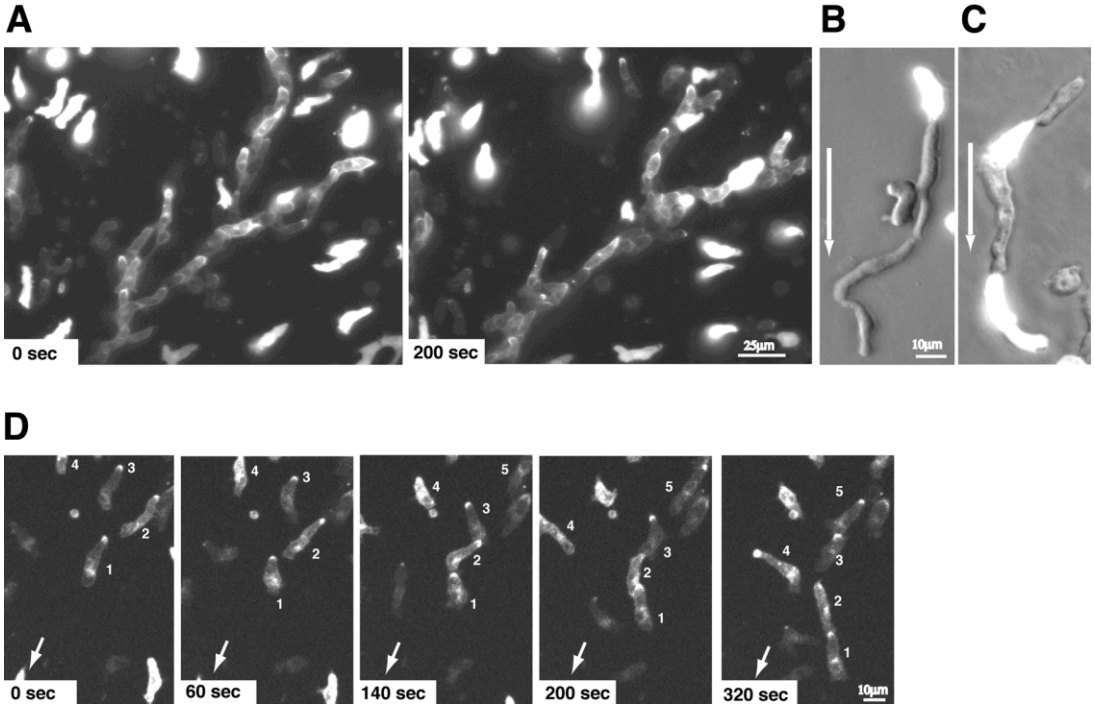

Figure 6. *aca*⁻ Cells Do Not Incorporate into Wild-Type Streams

(A) Fluorescent images depicting a mix of GFP/*aca*⁻ and ACA-YFP/*aca*⁻ cells. The GFP/*aca*⁻ cells appear white and the ACA-YFP/*aca*⁻ cells show their characteristic uropod staining. The tip of the micropipette is located just outside the left bottom corner of the frames. Also see Supplemental Movie S9 available at http://www.cell.com/cgi/content/full/112/4/549/DC1.

(B) Phase image of a mix of GFP/*aca*⁻ and wild-type AX3 cells as they stream. The image was taken with the fluorescent light on so that the GFP/*aca*⁻ cells appear white.

(C) Phase image of a mix of GFP/wild-type AX3 and ACA-YFP/*aca*⁻ cells as they stream. The image was taken as described in (B).

(D) Fluorescent images depicting ACA-YFP/*aca*⁻ cells as they are chemotaxing specifically to the back of cells ahead of them. The arrow represents the direction of the micropipette. Cells are individually numbered as they move up the gradient.

explain how cells stream. In this model, the release of cAMP from the posterior of the cells attracts and orients other cells so that they align in a head to tail fashion. To further explore this hypothesis, cell mixing experiments were performed where *aca*⁻ cells expressing GFP (GFP/*aca*⁻) were mixed with ACA-YFP/*aca*⁻ cells and exposed to a chemoattractant gradient. Figure 6A shows a montage of images taken from a representative mixing experiment (also see Supplemental Movie S9 available at http://www.cell.com/cgi/content/full/112/4/549/DC1). In these experiments, the micropipette is located just below the frames. While wild-type cells form long streams, the bright fluorescent GFP/*aca*⁻ cells are always migrating either alone, behind, or on top of an existing stream. Moreover, we did not observe wild-type or GFP/*aca*⁻ cells align at the rear of GFP/*aca*⁻ cells. In this regard, the *aca*⁻ cells clearly behave as stream terminators (Figure 6B). As a control, we mixed ACA-YFP/*aca*⁻ cells with GFP/wild-type AX3 cells and, as expected, found streams composed of both cell types (Figure 6C). Remarkably, when we studied how individual cells migrated to form streams, we noticed that they frequently chemotaxed specifically to the tail of the cell in front of them, often undergoing significant cytoskeletal rearrangements to do so (Figure 6D). These results support the notion that cAMP is released primarily from the uropod during chemotaxis and streaming.

In order to determine if the localization of ACA at the uropod of cells was essential for streaming, we asked whether *aca*⁻ cells expressing the constitutive mutant of ACA, which displays reduced uropod labeling, were capable of organizing into streams. Figures 7A and 7B show ACA-YFP/*aca*⁻ and ACA-C-YFP/*aca*⁻ cells just before and 20 min after they were placed in a gradient of chemoattractant. Compared to cells expressing wild-type ACA, the cells expressing the constitutive mutant showed severe streaming defects. As stated above, they did however respond and chemotax to the tip of the micropipette (see Supplemental Movie S10 available at above website). Because these cells have high basal adenylyl cyclase activity and are therefore constantly exposed to higher cAMP levels, we performed the same experiment with 10^{-5} M cAMP in the micropipette. Here again, the cells moved toward the tip of the micropipette but, as in the previous experiment, they showed a severe streaming defect (data not shown). These results strongly suggest that the streaming process is dependent not only on ACA, but most remarkably, on its proper cellular distribution to the uropod.

To further support our hypothesis stating that the uropod localization of ACA is essential for cells to stream, we set out to study the cellular distribution of ACA in cells lacking myosin II. Myosin II has been shown to be important for defining axial polarity and, based on our

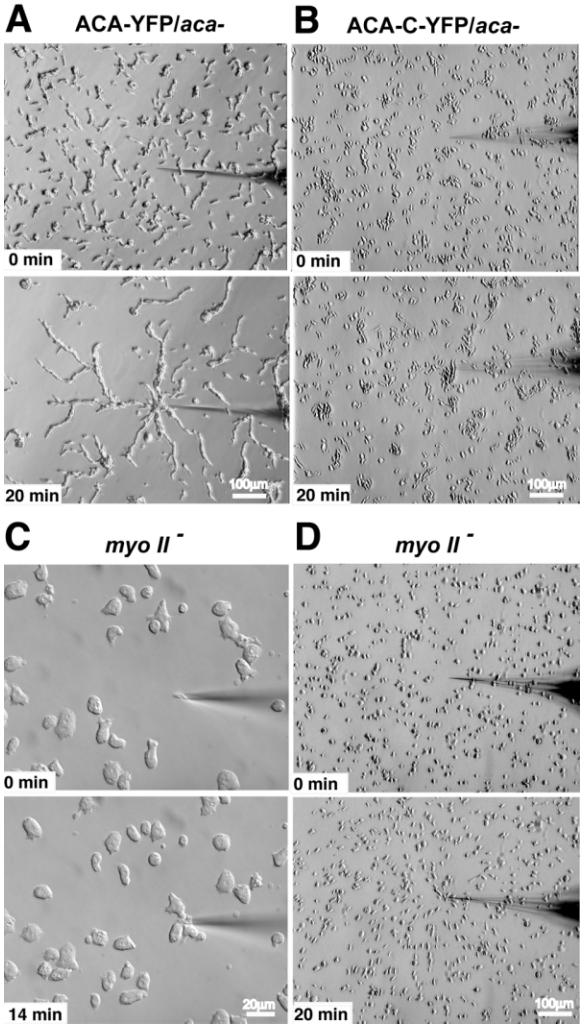

Figure 7. Cells with Reduced Enrichment of ACA-YFP at the Uropod Have Streaming Defects

(A) Images of ACA-YFP/*aca*$^-$ cells taken as the cells move toward a micropipette.

(B) Images of ACA-C-YFP/*aca*$^-$ cells taken as the cells move toward a micropipette. Also see Supplemental Movie S10 available at http://www.cell.com/cgi/content/full/112/4/549/DC1.

(C and D) High and low magnification images of *moyII*$^-$ cells taken as the cells are moving toward the micropipette. Also see Supplemental Movie S11 available at above website.

findings, we reasoned that ACA-YFP should be mislocalized in *myoII*$^-$ cells (Wessels et al., 1988). Figure 7C shows *myoII*$^-$ cells that were starved and pulsed with exogenous cAMP for 6 hr before and 14 min after being exposed to a chemoattractant gradient. As reported, the cells display severe polarity defects, yet they do chemotax, albeit slowly compared to wild-type cells (De Lozanne and Spudich, 1987; Wessels et al., 1988). We transformed *myoII*$^-$ cells with the ACA-YFP expression plasmid on several occasions, but were not successful in generating stable cell lines. We think that overexpression of ACA must be toxic to cells lacking myosin II. We nevertheless tested if *myoII*$^-$ cells were able to stream and found that, like *aca*$^-$ cells expressing the constitutive mutant of ACA, *myoII*$^-$ cells did not organize into streams (Figure 7D, see also Supplemental Movie S11 available at http://www.cell.com/cgi/content/full/112/4/549/DC1). Furthermore, when Shelden and Knecht (1995), performed cell mixing experiments, they found that *myoII*$^-$ cells migrated primarily at the lateral edges of wild-type streams and appeared to act as stream terminators. Taken together, these results strongly suggest that cellular polarity, and the asymmetric distribution of ACA that results from it, are required for cells to organize into streams.

Discussion

Synthesis and degradation of cAMP are tightly regulated phenomena. Like the *D. discoideum* adenylyl cyclase ACA, the nine G protein-coupled adenylyl cyclases expressed in mammalian cells are each predicted to consist of two sets of six transmembrane domains followed by large cytoplasmic loops where the catalytic and part of the regulatory domain reside. The mammalian enzymes are all activated by Gαs but exhibit complex responses to a variety of other regulators, including Gαi, G$\beta\gamma$, Ca^{2+}, and PKC (Hanoune and Defer, 2001). Crystallographic studies and site-directed mutagenesis have provided valuable information on the catalytic and regulatory mechanisms that govern adenylyl cyclase activation (Hurley, 1999; Tesmer and Sprang, 1998). This said, very little is actually known about the cellular localization of adenylyl cyclases in the context of specific physiological processes.

We show here that ACA is highly enriched at the uropod of chemotaxing cells and is essential for cells to align in a head to tail fashion to form streams. This finding brings forth a unique mechanism to explain how groups of cells use signal relay to amplify chemotactic responses. Several lines of evidence suggest that streaming is mediated by cAMP secreted at the back of chemotaxing cells, where ACA is enriched. First, *aca*$^-$ cells and *aca*$^-$ cells expressing a G protein-uncoupled mutant of ACA do not stream. Second, *aca*$^-$ cells expressing a constitutive mutant of ACA, which displays a reduced enrichment at the uropod of cells, also present a severe streaming defect. Third, when mixed with wild-type cells, *aca*$^-$ cells act as stream terminators. Finally, wild-type cells migrate specifically to the back of cells ahead of them. Taken together, these results establish that ACA needs to be responsive to an external stimulus and be properly localized for streaming to take place. It therefore follows that the uropod must be the site where cAMP is secreted. We cannot rule out that in addition to acting as a chemoattractant, cAMP could also regulate adhesion. It has indeed been reported that cellular adhesion plays a role in the streaming process later in development (Gomer, 2001).

The fact that the essential cytosolic regulator of ACA, CRAC, translocates specifically at the leading edge of chemotaxing cells appears paradoxical when envisioning the mechanisms that regulate ACA activity (Parent et al., 1998). We originally surmised that ACA would behave like chemoattractant receptors and show a uniform distribution. In this scenario, the enzyme would be available all over the cell periphery and simply wait for CRAC to translocate and act upon it. When the kinetics

of ACA activation and CRAC translocation are compared, the crest of CRAC translocation is seen to occur ~60 s before ACA activity peaks (Parent et al., 1998). This suggests that there may be additional steps between CRAC translocation and ACA activation. Indeed, the activation of ACA requires, in addition to the Gβγ subunits and CRAC, the MAP kinase ERK2, components of the Ras pathway, and the cytosolic regulator Pianissimo (Chen et al., 1997; Lim et al., 2001; Segal et al., 1995). It is thus entirely possible that the activation pathway is initiated at the front of cells and culminates at the back where cAMP relays the signal to surrounding cells. Remarkably, this is not the only instance where a regulator and its effector do not colocalize: the activation of the serine/threonine kinase PAKa, which is localized at the uropod of cells, requires PKB, which like CRAC localizes to the leading edge of chemotaxing cells (Chung et al., 2001b). Therefore, it appears that an activating cascade beginning at the front of cells and culminating at the back could be common to a variety of responses.

The mechanisms responsible for ACA localization to the uropod depend on the actin cytoskeleton and the establishment of polarity, raising the possibility that ACA might interact with cytoskeletal proteins. Although we have yet to determine this, we do know that ACA's localization does not depend on the presence of its regulator CRAC and that CRAC is properly localized to the leading edge when expressed in *aca*$^-$ cells. Similarly, the uncoupled mutant of ACA, which does not respond to G protein stimulation and is therefore phenotypically equivalent to *crac*$^-$ cells in regards to ACA activation, is clustered in polarized cells. Surprisingly, however, the constitutive mutant of ACA does display an aberrant cellular distribution, where the extent of uropod enrichment is dramatically reduced and the amount of vesicle labeling is proportionally increased compared to the wild-type enzyme. This suggests that the state of activation of ACA is important for its cellular localization. Since the uncoupled mutant was properly localized, the aberrant distribution of the constitutive mutant can be interpreted in either of two ways. First, it could imply that the localization is somehow dependent on the amount of cAMP present. In this scenario, the constant presence of cAMP would lead to a high turnover of vesicle trafficking between the plasma membrane and intracellular pools. Our results show that PKA, the main cellular target of cAMP, is however not involved. Alternatively, the signaling events leading to the shut down of ACA activity, the adaptation response, could be important in the regulation of the cellular distribution of ACA.

The restricted cellular distribution of ACA in polarized cells brings forward insights into the spatial and temporal regulation of signaling in the context of complex cellular responses. The compartmentalization of cAMP signaling has been suggested to occur in a variety of cell types. By using cyclic nucleotide-gated channels as reporters for cAMP, Rich et al. (2000) found that the channels colocalize with adenylyl cyclases within regions of restricted cAMP diffusion. Similarly, using FRET technology, microdomains with increased concentrations of cAMP have been observed in cardiac myocytes (Zaccolo and Pozzan, 2002). Although it has yet to be shown for neutrophils, it has been proposed that the compartmentalization of cAMP metabolism could also exist in these cells (Harvath et al., 1991). Our findings now show the dynamic nature of the cellular distribution of adenylyl cyclases and bring forward an added layer of complexity to the regulation of signaling events in the context of cellular responses. Our data strongly suggest that the polarized, asymmetric cellular distribution of ACA is essential for cells to stream. In addition, the fact that we find adenylyl cyclases on dynamic vesicular structures brings forward the intriguing possibility that trafficking of adenylyl cyclases between plasma membrane and internal vesicle pools occurs and that this is an integral part of the regulatory mechanisms that govern enzyme activity.

Our findings reveal mechanisms that will have impact on two fronts. First, the asymmetric distribution of ACA on the plasma membrane as well as its presence on intracellular vesicles shows that cells have the capacity to target adenylyl cyclases to specific cellular domains. This distribution would then be primed to generate cellular compartments where cAMP synthesis is spatially confined. We anticipate that this type of behavior will also be observed with mammalian adenylyl cyclases in a variety of physiological responses thereby providing an added layer of intricacy to this major signaling cascade. In this regard, Cioffi and collaborators recently visualized the cellular distribution of the Type VIII adenylyl cyclase in endothelial cells. They found plasma membrane labeling that was enriched at cell-cell borders and suggested that this distribution could explain how localized changes in calcium-dependent cAMP concentrations regulate intercellular gap formation (Cioffi et al., 2002). Second, we envision that the signal relay mechanism that *D. discoideum* amoebae use to amplify the chemotactic response and stream is common to other cell types. We propose that the amplification response is instigated the moment cells are exposed to chemoattractants, which causes cells to polarize and become motile. Indeed, our data show that the acquisition of cellular polarity and the asymmetric distribution of ACA necessitate chemoattractant receptor stimulation, whether the chemoattractant is added uniformly—as in chemokinesis—or when presented as a gradient. This then initiates a series of events that lead to the asymmetric distribution to the uropod of the components responsible for the generation of chemoattractants—ACA in the case of *D. discoideum*—and the amplification of the chemotactic response and the formation of streams. Like *D. discoideum* amoebae, leukocytes have been shown to secrete chemoattractants in response to chemoattractant stimulation (Crooks and Stockley, 1998). It is therefore enticing to speculate that leukocytes as they make their way to sites of inflammation, keratinocytes in the process of wound repair, or migrating cells in the developing embryo all use signal relay to amplify their chemotactic response.

Experimental Procedures

ACA-YFP Fusion Protein Construct and Transformation

The EYFP gene was amplified from the Living Colors pEYFP vector (BD Biosciences, Franklin Lake, NJ) and cloned at the 3′ end of the ACA cDNA. The resulting ACA-YFP fusion was sequenced and cloned into the *D. discoideum* expression vectors B18 and CV5,

which give rise to constitutive levels of expression (Johnson et al., 1991). The ACA-YFP plasmid was electroporated into *D. discoideum* cells as previously described using a Bio-Rad gene pulser (Howard et al., 1988; Pitt et al., 1992). Cells stably expressing ACA-YFP were selected in media containing 5 or 20 μg/ml G418. ACA-YFP clones were obtained by plating transformants on *Kleibsiella aerogenes* lawns (Sussman, 1987). The developmental phenotype of the clones was determined by plating them on non-nutrient agar at 22°C, as described by Devreotes et al. (1987).

Cell Culture and Development

Wild-type, *aca*$^-$, *crac*$^-$, *pkacat*$^-$, *and myoII*$^-$ cells were grown to ~5×10^6 cells/ml in HL5 media (Mann et al., 1992; Pitt et al., 1992; Insall et al., 1994; Ruppel et al., 1994). They were harvested by centrifugation, washed once in DB (5 mM Na_2HPO_4, 5 mM NaH_2PO_4 [pH 6.2], 2 mM $MgSO_4$, and 200 μM $CaCl_2$), and finally resuspended at 2×10^7 cells/ml. To allow differentiation, the cells were shaken at 100 rpm for 4–7 hr with repeated pulses of 75 nM cAMP (Devreotes et al., 1987; Parent and Devreotes, 1996a). The cells were then processed according to the assay performed.

Sub-Cellular Fractionation and Immunoblotting

Cells were differentiated for 5 hr, resuspended in DB at 4×10^7 cells/ml, and lysed through 5 μm nucleopore filters. The lysates were centrifuged and the pellets were resuspended in Laemmli buffer (Laemmli, 1970). Whole-cell, pellet, and supernatant samples were subjected to 7% SDS-PAGE analysis and transferred to Immobilon-P. The Immobilon-P was blotted with anti-GFP monoclonal antibody and detection was performed by chemiluminescence using a donkey anti-mouse horseradish peroxidase-coupled antibody (Amersham, Arlington Heights, IL)

Adenylyl Cyclase Assays

Adenylyl cyclase activity was assayed as previously described (Parent and Deveotes, 1995).

Fluorescence Microscopy

Cells were differentiated as described above. Samples were spotted on Lab-Tek chambered cover slips (Nunc, Naperville, IL), left for 5 min, and covered with PB. They were viewed with a Zeiss Axiovert S100 microscope (Thornwood, NY) equipped with automated filter wheels (Ludl Electronic Products, Hawthrone, NJ). Images were recorded with a CoolSnap PXL CCD camera (Roper, Trenton, NJ) operated by the IPLab software (Scanalytics, Fairfax, VA). All images in a series were processed identically using IPLab and Adobe Photoshop.

Confocal Microscopy

Cells were prepared for microscopy as described above and were observed with a Zeiss Axiovert 135TV microscope equipped with a Perkin-Elmer Ultraview "spinning wheel" confocal system. Single plane images and Z stacks were taken with an Orca-ERII CCD camera (Hamamatsu, Bridgewater, NJ).

Immunofluorescence

Cells expressing wild-type ACA were fixed at room temperature for 10 min in 1% formaldehyde (EM Grade, Ted Pella), 0.1% glutaraldehyde (EM Grade, Ted Pella), and 0.01% Triton in PB. After blocking in PB with 10% FBS and 2% normal goat serum, the cells were incubated with anti-ACA polyclonal antibody (1:100) followed by goat anti-rabbit antibody conjugated to Alexa 568 (1:2500) (Molecular Probes, Eugene OR) (Parent and Deveotes, 1995). ACA cellular localization was visualized as described above.

Chemotaxis Assays

The chemotaxis assays were performed as previously described (Parent et al., 1998). Briefly, differentiated cells were prepared for analysis as described. Gradients were generated using a microinjector connected to micropipettes containing 1 μM cAMP (Femtotips, Eppendorf, Germany). The needle was placed into the chambered cover slips and images were captured at specified times.

Quantitative Analysis of Fluorescence Intensity

A confocal stack was taken through the entire cell using the UltraView spinning disk confocal system. A maximum intensity projection was made of the center sections; sections were not used if the plasma membrane overlapped the cytoplasm of the previous section. To measure the total fluorescence in the uropod, an area was outlined on the uropod membrane and the fluorescence intensity of all pixels within the designated area was summed together. If the ACA-YFP construct being expressed was polarized, that section of the uropod was marked and quantified. If the ACA-YFP construct expression was not polarized, an average stretch of uropod membrane was marked and quantified. These numbers were used to compare the total uropod fluorescence in cells expressing wild-type ACA-YFP and to that of cells expressing ACA-C-YFP. Additionally, in each cell the total fluorescence in the uropod was compared to the total fluorescence in an equal area outlined in the front of the cell. This ratio was used to compare the polarization of the ACA-YFP constructs.

Cell Mixing Experiments

ACA-YFP/*aca*$^-$ and GFP/*aca*$^-$ cells were pulsed as described above. After 5 hr, the two cells lines were mixed (75% ACA-YFP/*aca*$^-$ cells and 25% GFP/*aca*$^-$ cells), spotted on a chambered slide, and a cAMP-containing micropipette was placed into the chamber and activated. Streams were allowed to develop and visualized using both phase and fluorescence microscopy.

Acknowledgments

We thank Drs. Richard A. Firtel and Edward D. Korn for providing the *pkacat*$^-$ and *myoII*$^-$ cells, respectively. We also thank Drs. Pierre A. Coulombe, Frank I. Comer, and Dana C. Mahadeo as well as Christopher Lippincott and Rory L. Smoot for helpful discussions and support. We are also grateful to Dr. Alan Kimmel and members of his group for excellent suggestions and stimulating discussions.

Received: September 4, 2002
Revised: January 22, 2003

References

Anjard, C., van Bemmelen, M., Veron, M., and Reymond, C.D. (1997). A new spore differentiation factor (SDF) secreted by *Dictyostelium* cells is phosphorylated by the camp dependent protein kinase. Differentiation *62*, 43–49.

Aubry, L., and Firtel, R.A. (1999). Integration of signaling networds that regulate *Dictyostelium* differentiation. Annu. Rev. Cell. Dev. Biol. *15*, 469–517.

Brickey, D.A., Naranan, V., Sucic, J.F., and Rutherford, C.L. (1990). Regulation of the two forms of glycogen phosphorylase by cAMP and its analogs in *Dictyostelium discoideum*. Mol. Cell. Biochem. *97*, 17–33.

Chen, M.Y., Long, Y., and Devreotes, P.N. (1997). A novel cytosolic regulator, Pianissimo, is required for chemoattractant receptor and G protein-mediated activation of the 12 transmembrane domain adenylyl cyclase in *Dictyostelium*. Genes Dev. *11*, 3218–3231.

Chung, C.Y., Funamoto, S., and Firtel, R.A. (2001a). Signaling pathways controlling cell polarity and chemotaxis. Trends Biochem. Sci. *26*, 557–566.

Chung, C.Y., Potikyan, G., and Firtel, R.A. (2001b). Control of cell polarity and chemotaxis by Akt/PKB and PI3 kinase through the regulation of PAKa. Mol. Cell *7*, 937–947.

Cioffi, D.L., Moore, T.M., Schaack, J., Creighton, J.R., Cooper, D.M., and Stevens, T. (2002). Dominant regulation of interendothelial cell gap formation by calcium-inhibited type 6 adenylyl cyclase. J. Cell Biol. *157*, 1267–1278.

Crooks, S.W., and Stockley, R.A. (1998). Leukotriene B4. Int. J. Biochem. Cell Biol. *30*, 173–178.

De Lozanne, A., and Spudich, J.A. (1987). Disruption of the *Dictyostelium* myosin heavy chain gene by homologous recombination. Science *236*, 1086–1091.

Devreotes, P., Fontana, D., Klein, P., Sherring, J., and Theibert, A. (1987). Transmembrane signaling in *Dictyostelium*. Methods Cell Biol. *28*, 299–331.

Gomer, R.H. (2001). Not being the wrong size. Nat. Rev. Mol. Cell Biol. *2*, 48–54.

Hanoune, J., and Defer, N. (2001). Regulation and role of adenylyl cyclase isoforms. Annu. Rev. Pharmacol. Toxicol. *41*, 145–174.

Harvath, L., Robbins, J.D., Russell, A.A., and Seamon, K.B. (1991). cAMP and human neutrophil chemotaxis. Elevation of cAMP differentially affects chemotactic responsiveness. J. Immunol. *146*, 224–232.

Hauert, A.B., Martinelli, S., Marone, C., and Niggli, V. (2002). Differentiated HL-60 cells are a valid model system for the analysis of human neutrophil migration and chemotaxis. Int. J. Biochem. Cell Biol. *34*, 1467–1472.

Howard, P.K., Ahern, K.G., and Firtel, R.A. (1988). Establishment of a transient expression system for *Dictyostelium discoideum*. Nucleic Acids Res. *16*, 2613–2623.

Hurley, J.H. (1999). Structure, mechanism, and regulation of mammalian adenylyl cyclase. J. Biol. Chem. *274*, 7599–7602.

Insall, R., Kuspa, A., Lilly, P.J., Shaulsky, G., Levin, L.R., Loomis, W.F., and Devreotes, P.N. (1994). CRAC, a cytosolic protein containing a pleckstrin homology domain, is required for receptor and G protein-mediated activation of adenylyl cyclase in *Dictyostelium*. J. Cell Biol. *126*, 1537–1545.

Jin, T., Zhang, N., Long, Y., Parent, C.A., and Devreotes, P.N. (2000). Localization of the G protein $\beta\gamma$ complex in living cells during chemotaxis. Science *287*, 1034–1036.

Johnson, R.L., Vaughan, R.A., Caterina, M.J., van Haastert, P.J.M., and Devreotes, P.N. (1991). Overexpression of the cAMP receptor 1 in growing *Dictyostelium* cells. Biochemistry *30*, 6982–6986.

Laemmli, U.K. (1970). Cleavage of structural proteins during the assembly of the head of bacteriophage T4. Nature *227*, 680–685.

Lilly, P.J., and Devreotes, P.N. (1995). Chemoattractant and GTPγS-mediated stimulation of adenylyl cyclase in *Dictyostelium* requires translocation of CRAC to membranes. J. Cell Biol. *129*, 1659–1665.

Lim, C.J., Spiegelman, G.B., and Weeks, G. (2001). RasC is required for optimal activation of adenylyl cyclase and Akt/PKB during aggregation. EMBO J. *20*, 4490–4499.

Mann, S.K.O., Yonemoto, W.M., Taylor, S.S., and Firtel, R.A. (1992). *DdPK3*, which plays essential roles during *Dictyostelium* development, encodes the catalytic subunit of cAMP-dependent protein kinase. Proc. Natl. Acad. Sci. USA *89*, 10701–10705.

Mann, S.K.O., Brown, J.M., Briscoe, C., Parent, C., Pitt, G., Devreotes, P.N., and Firtel, R.A. (1997). Role of cAMP-dependent protein kinase in controlling aggregation and postaggregative development in *Dictyostelium*. Dev. Biol. *183*, 208–221.

Meili, R., Ellsworth, C., Lee, S., Reddy, T.B., and Firtel, R.A. (1999). Chemoattractant-mediated transient activation and membrane localization of Akt/PKB is required for efficient chemotaxis to cAMP in *Dictyostelium*. EMBO J. *18*, 2092–2105.

Parent, C.A., and Deveotes, P.N. (1995). Isolation of inactive and G protein-resistant adenylyl cyclase mutants using random mutagenesis. J. Biol. Chem. *270*, 22693–22696.

Parent, C.A., and Devreotes, P.N. (1996a). Constitutively active adenylyl cyclase mutant requires neither G proteins nor cytosolic regulators. J. Biol. Chem. *271*, 18333–18336.

Parent, C.A., and Devreotes, P.N. (1996b). Molecular genetics of signal transduction in *Dictyostelium*. Annu. Rev. Biochem. *65*, 411–440.

Parent, C.A., Blacklock, B.J., Froehlich, W.M., Murphy, D.B., and Devreotes, P.N. (1998). G protein signaling events are activated at the leading edge of chemotactic cells. Cell *95*, 81–91.

Parent, C.A., and Devreotes, P.N. (1999). A cell's sense of direction. Science *284*, 765–770.

Pitt, G.S., Milona, N., Borleis, J.A., Lin, K.C., Reed, R.R., and Devreotes, P.N. (1992). Structurally distinct and stage-specific adenylyl cyclase genes play different roles in *Dictyostelium* development. Cell *69*, 305–315.

Pitt, G.S., Brandt, R., Lin, K.C., Devreotes, P.N., and Schaap, P. (1993). Extracellular cAMP is sufficient to restore developmental gene expression and morphogenesis in *Dictyostelium* cells lacking the aggregation adenylyl cyclase (ACA). Genes Dev. *7*, 2172–2180.

Rich, T.C., Fagan, K.A., Nakata, H., Schaack, J., Cooper, D.M., and Karpen, J.W. (2000). Cyclic nucleotide-gated channels colocalize with adenylyl cyclase in regions of restricted cAMP diffusion. J. Gen. Physiol. *116*, 147–161.

Ruppel, K., Uyeda, T.Q.P., and Spudich, J.A. (1994). Role of a highly conserved lysine 130 of myosin motor domain. In vivo and in vitro characterization of site specifically mutated myosin. J. Biol. Chem. *269*, 18773–18780.

Segal, J.E., Kuspa, A., Shaulsky, G., Ecke, M., Maeda, M., Gaskins, C., Firtel, R.A., and Loomis, W.F. (1995). A MAP kinase necessary for receptor-mediated activation of adenylyl cyclase in *Dictyostelium*. J. Cell Biol. *128*, 405–413.

Servant, G., Weiner, O.D., Neptune, E.R., Sedat, J.W., and Bourne, H.R. (1999). Dynamics of a chemoattractant receptor in living neutrophils during chemotaxis. Mol. Biol. Cell *10*, 1163–1178.

Servant, G., Weiner, O.D., Herzmark, P., Balla, T., Sedat, J.W., and Bourne, H.R. (2000). Polarization of chemoattractant receptor signaling during neutrophil chemotaxis. Science *287*, 1037–1040.

Shelden, E., and Knecht, D.A. (1995). Mutants lacking myosin II cannot resist forces generated during multicellular morphogenesis. J. Cell Sci. *108*, 1105–1115.

Sussman, M. (1987). Cultivation and synchronous morphogenesis of *Dictyostelium* under controlled experimental conditions. Methods Cell Biol. *28*, 9–29.

Tesmer, J.J.G., and Sprang, S.R. (1998). The structure, catalytic mechanism and regulation of adenylyl cyclase. Curr. Opin. Struct. Biol. *8*, 713–719.

van Ments-Cohen, M., and van Haastert, P.J.M. (1989). The cyclic nucleotide specificity of eight cAMP-binding proteins in *Dictyostelium discoideum* is correlated into three groups. J. Biol. Chem. *264*, 8717–8722.

Wessels, D., Soll, D.R., Knecht, D., Loomis, W.F., De Lozanne, A., and Spudich, J. (1988). Cell motility and chemotaxis in *Dictyostelium* amoebae lacking myosin heavy chain. Dev. Biol. *128*, 164–177.

Wu, L., Valkema, R., van Haastert, P.J.M., and Devreotes, P.N. (1995). The G protein β subunit is essential for multiple responses to chemoattractants in *Dictyostelium*. J. Cell Biol. *129*, 1667–1675.

Xiao, Z., Zhang, N., Murphy, D.B., and Devreotes, P.N. (1997). Dynamic distribution of chemoattractant receptors in living cells during chemotaxis and persistent stimulation. J. Cell Biol. *139*, 365–374.

Zaccolo, M., and Pozzan, T. (2002). Discrete microdomains with high concentration of cAMP in stimulated rat neonatal cardiac myocytes. Science *295*, 1711–1715.

Zigmond, S.H., Levitsky, H.I., and Kreel, B.J. (1981). Cell polarity: an examination of its behavioral expression and its consequences for polymorphonuclear leukocyte chemotaxis. J. Cell Biol. *89*, 585–592.